



## UvA-DARE (Digital Academic Repository)

### Physiological studies to optimize growth of the prototype biosolar cell factory *Synechocystis* sp. PCC6803

van Alphen, P.

**Publication date**

2017

**Document Version**

Other version

**License**

Other

[Link to publication](#)

**Citation for published version (APA):**

van Alphen, P. (2017). *Physiological studies to optimize growth of the prototype biosolar cell factory Synechocystis* sp. PCC6803. [Thesis, fully internal, Universiteit van Amsterdam].

**General rights**

It is not permitted to download or to forward/distribute the text or part of it without the consent of the author(s) and/or copyright holder(s), other than for strictly personal, individual use, unless the work is under an open content license (like Creative Commons).

**Disclaimer/Complaints regulations**

If you believe that digital publication of certain material infringes any of your rights or (privacy) interests, please let the Library know, stating your reasons. In case of a legitimate complaint, the Library will make the material inaccessible and/or remove it from the website. Please Ask the Library: <https://uba.uva.nl/en/contact>, or a letter to: Library of the University of Amsterdam, Secretariat, P.O. Box 19185, 1000 GD Amsterdam, The Netherlands. You will be contacted as soon as possible.

## 6 **Culturing of *Synechocystis* sp. PCC6803 with N<sub>2</sub>/CO<sub>2</sub> in a diel regime shows multi-phase glycogen dynamics and low maintenance costs**

S. Andreas Angermayr\*, Pascal van Alphen\*, Dicle Hasdemir, Gertjan Kramer, Muzamal Iqbal, Wilmar van Grondelle, Huub C. Hoefsloot, Young Hae Choi, Klaas J. Hellingwerf

\* Authors contributed equally to this work

### **Abstract**

Investigating the physiology of cyanobacteria cultured under a diel light regime is relevant for a better understanding of the resulting growth characteristics and for specific biotechnological applications that are foreseen for these photosynthetic organisms. Here, we present the results of a multi-omics study of the model cyanobacterium *Synechocystis* sp. PCC6803, cultured in a lab-scale photobioreactor in physiological conditions relevant for large-scale culturing. The culture is sparged with N<sub>2</sub> and CO<sub>2</sub>, leading to an anoxic environment during the dark period. Growth follows the availability of light. Metabolite analysis performed with <sup>1</sup>H Nuclear Magnetic Resonance analysis, shows that amino acids involved in nitrogen and sulfur assimilation show elevated levels in the light. Most protein levels, analyzed through mass spectrometry, remain rather stable. However, several high-light-response proteins and stress-response proteins show distinct changes at the onset of the light period. Microarray-based transcript analysis finds common patterns of ~56 % of the transcriptome following the diel regime. These oscillating transcripts can be grouped coarsely into genes that are up-regulated and down-regulated in the dark period, respectively. The accumulated glycogen is degraded in the anaerobic environment in the dark. A small part is degraded gradually, reflecting basic maintenance requirements of the cells in darkness. Surprisingly, the largest part is degraded rapidly in a short time span at the end of the dark period. This degradation could allow rapid formation of metabolic intermediates at the end of the dark period, preparing the cells for the resumption of growth at the start of the light period.

This chapter was published as:

**Angermayr, SA\*, P van Alphen\*, D Hasdemir, G Kramer, M Iqbal, W van Grondelle, HC Hoefsloot, YH Choi, KJ Hellingwerf.** 2016. Culturing *Synechocystis* sp. Strain PCC 6803 with N<sub>2</sub> and CO<sub>2</sub> in a Diel Regime Reveals Multiphase Glycogen Dynamics with Low Maintenance Costs. *Applied and environmental microbiology*. 82:4180-4189.

## 6.1 Introduction

Understanding cyanobacterial physiology in a diel environment is of interest to understand circadian regulation in general and for the utilization of these organisms in biotechnological applications. Our exploration of the effect of a diel light cycle on a cyanobacterial culture started with the wish to investigate the response of the cells' metabolic network to the imposed repetitively fluctuating environment, considering future biotechnological applications. The attractiveness of employing a photosynthetic organism in industrial biotechnology is that it can harness the energy from the sun, even though this energy is available only in a dilute and intermittent fashion. Utilizing cyanobacteria for large-scale product formation will benefit from a high cell density provided the trade-off of self-shading stays within reasonable bounds. Industrial-scale cultures of cyanobacteria growing in large-scale closed photobioreactors are envisioned to be fed by CO<sub>2</sub>-rich exhaust gases from combustion engines and/or anaerobic digesters. Such culturing conditions may result in a microaerobic or an anoxic environment when photosynthesis stops in darkness.

Most biotechnological applications of cyanobacteria are based on the use of synthetic biology to re-route intermediary metabolism, such that heterologous production pathways allow formation of a preferred product 251. Intermediary metabolism forms a highly interconnected network, initiated by nutrient influx and governed by multiple layers of regulation. Whether engineered metabolic routes result in high rates of product formation depends on the metabolic flux capacities, proper regulatory signals and the availability of the intracellular substrate(s). Hence, the productivity of cyanobacteria is highly dependent on the changes of their metabolite levels and/or regulation of metabolism during the daily cycle (71, 252-254). Rhythms of the metabolism are affected by the light/dark transitions but also by the circadian clock, both with distinct effects (255). Disentangling those influences will benefit the optimization of cyanobacterial production systems. Cyanobacteria, such as *Synechocystis* sp. PCC6803 (hereafter: *Synechocystis*) are oxygenic photoautotrophic microorganisms that can be modified to produce a wide range of products (256-258). Accordingly, CO<sub>2</sub> can be invested, via the cyanobacterial metabolism, as the carbon substrate for sustainable production of biofuels, bulk chemicals, etc., thus generating CO<sub>2</sub>-neutral energy carriers and commodity chemicals (22). Consequently, there is an interest in the large-scale growth of these organisms, in the compounds contained in their biomass, as well as in compounds excreted into the growth medium (259). So far, excreted products, synthesized via heterologous pathways, typically are precursors to bioplastics (e.g. butane-diol and lactic acid (68, 74)), biofuels (e.g. ethanol and butanol) (260) and secondary metabolites and flavor compounds such as vitamins and terpenes (261, 262).

In this study, wild type *Synechocystis* cells were grown in continuous culture in a turbidostat-controlled lab-scale photobioreactor, sparged with a mixture of N<sub>2</sub> and CO<sub>2</sub> (249). The culture was subjected to a diel rhythm of 12 hours light, 12 hours darkness

(LD), which resulted in rapid oxygen depletion during the dark period. These are conditions that mimic the conditions of mass culturing in a large-scale closed photobioreactor, equipped with a degassing system and sparged with off-gases originating from the combustion of fossil fuel (263) or an anaerobic digester (264). To achieve high cell densities, high light intensities are needed which, depending on geographical location, may regularly exceed the cells photosynthetic capacity (especially at mid-day in full sunlight). Such a changing environment, specifically with respect to the primary source of energy (light), and the lack of oxygen in the dark period, may have a strong influence on the metabolic state and metabolic efficiency of cyanobacteria; the organism for instance will have to react to the anoxic environment by fermentation, to cover the energy requirement for cellular maintenance (252, 265).

To understand these physiological responses in more detail, we set out to investigate the metabolome, proteome and transcriptome of such cells from samples taken at time points close to the changes of light availability, to study the immediate response and subsequent adaptation to the diel regime. The most striking observations that were made will be discussed in detail.

## **6.2 Materials and Methods**

### **6.2.1 Strain and pre-culture conditions**

A pre-culture of the glucose tolerant wild type strain of *Synechocystis* sp. PCC6803 (strain obtained from D. Bhaya, Stanford) was incubated in BG-11 medium (Sigma, St. Louis, MO, USA) and grown at 30 °C in a shaking incubator at 120 rpm (Innova 43, New Brunswick Scientific, Enfield, CT, USA). Cultures were illuminated with constant moderate light provided by 15 W cool fluorescent white lights (F15T8-PL/AQ, General Electric, CT, USA). The resulting light intensity was 30  $\mu\text{mol photons/m}^2/\text{s}$  measured with a LI-250 light meter (LI-COR, Lincoln, NE, USA). Prior to the experiments in the photobioreactor (see below), a 100 ml pre-culture was cultivated in BG-11 medium in a 300 ml Erlenmeyer flask. To assure that an axenic culture was used, an aliquot of the culture was spread on BG-11 plates and on LB plates (solidified with 1.5 % w/v agar). Plates were incubated at 30 °C and screened for three consecutive days for potential contaminants. BG-11 plates were supplemented with 10 mM TES-KOH (pH 8), 5 mM glucose and 0.3 % sodium thiosulfate.

### **6.2.2 Photobioreactor (PBR)**

The *Synechocystis* pre-culture (see above) was used to seed two FMT-150 photobioreactors (Photon System Instruments, Brno, Czech Republic, hereafter PBR) with 100 ml culture each. This study makes use of the ~1 L vessel model FMT-150, that is temperature controlled and illuminated from one side by blue- and red-light emitting diodes (LEDs) (249). Growth was monitored by the integrated densitometer as optical density measured at 735 nm ( $\text{OD}_{735}$ ). Culture medium was BG-11 (Sigma). Continuous gas mixing was provided by the Gas Mixing System GMS150 (Photon System Instruments, Brno, Czech Republic) set to 0.5 % CO<sub>2</sub> / 99.5 % N<sub>2</sub>, coupled to mass flow controllers (Smart Mass Flow Model 5850S, Brooks Instruments, PA, USA) to supply 0.5 l/min to each

PBR. The CO<sub>2</sub> influx provided an excess of (inorganic) carbon and clamped the pH in the preferred range of 7.5-8.0. The temperature was kept at 30 ± 1 °C. The lid of the PBRs accommodated a pH electrode, a Clark-type dissolved dO<sub>2</sub> electrode and potentiometric dissolved dCO<sub>2</sub> electrode (Mettler-Toledo).

The light regime applied by the LED board provided 12 hours illumination and 12 hours darkness in square-wave cycles (LD). The culture was kept at OD<sub>735</sub> of 0.8 ± 0.01, as measured by the integrated densitometer at 735 nm and regulated by turbidostat control. This value corresponds to ~2.57 ± 0.05 as determined at OD<sub>730</sub> in a bench-top spectrophotometer with 1 cm path length (Lightwave II, Biochrom, Cambridge, UK) and this was kept constant over multiple consecutive days of LD regime (Supplemental Material, **Fig. S1-4**). The pump coupled to the turbidostat control attached to the medium reservoir was set to 5.6 ml/min, resulting in a 'saw-tooth' pattern in the OD reading from the repetitive influx of medium when the upper bound of the threshold is reached until the medium pump is stopped again at the lower bound. The slope in-between the pump intervals was used to determine the growth rate. The two vessels were illuminated with LED arrays consisting of blue (445 nm, 18 nm full width at half maximum (FWHM), and 458 nm, 16 nm FWHM, respectively) and red (for both PBRs: 636 nm, 20 nm FWHM) LEDs (249). The LED boards provided 500 μmol photons/m<sup>2</sup>/s of each wavelength to the culture vessels. Less than 5 % of the light-input was measured at the opposite side of each vessel, probably implying a light-limited growth regime for the whole population (149).

After an initial period of continuous illumination, to reach the target cell density rapidly (i.e. a couple of days), the LD regime was applied over a period of one week, until a quasi-steady-state was reached. Quasi-steady-state was judged from the optical density measurements and visual inspection of the recurring patterns of OD<sub>735</sub> and OD<sub>680</sub>, the ratio of which was used as a measure for chlorophyll content (Supplemental Material, **Fig. S2**). Next, over a period of 10 consecutive days, samples were taken for metabolite analysis. Thereafter, within three consecutive 24-hour periods samples for protein analysis, glycogen determination, and dry cell weight (gram dry weight, gDW) determination were taken (for sampling time points see **Fig. 6.1** and **S1**). The repetitive signal-output patterns of the two PBR systems (OD<sub>735</sub>, OD<sub>680</sub>, dO<sub>2</sub>, dCO<sub>2</sub>, pH and temperature) were essentially identical for the whole duration of the experiment (Supplemental Material, **Fig. S2-4**). The dO<sub>2</sub> and the OD<sub>680</sub> signal showed slightly decreasing amplitude during the initial 1-week period that was used to establish a quasi-steady-state. This signal stabilized, however, before the sampling took place (Supplemental Material, **Fig. S2A** and **S3**).

For growth rate determination, a best fit based on an exponential equation was derived from the OD<sub>735</sub> signal, in between the pre-set thresholds for the turbidostat control, which controls the supply of fresh medium (Supplemental Material, **Fig. S2**). For the identification of the first actual growth phase after the shift to the light period the lower threshold effectively indicates the end of the lag phase. It should be noted that the rapid drop of the OD<sub>735</sub> signal at the onset of the dark period is an artifact of the optical-density

measurement, caused by the temperature change of the equipment, due to switching-off of the light (data not shown). Likewise, the rapid increase of the OD<sub>735</sub> signal at the onset of illumination is caused by the reverse effect.

For the metabolite analysis 50 ml cell suspension was harvested for each NMR-sample (~18 mg dry weight). Sampling five times per 24 h period results in the removal of 250 ml of culture (from a total of 1 L), which still allows a stable growth regime over multiple subsequent days (Supplemental Material, **Fig. S2-4**). About 270-300 ml of new medium is pumped-in each 24 h period which, under this chosen regime, compensates for the removal of culture and allows for the continuous culturing. We selected 9 (PBR1) and 10 (PBR2) consecutive days for NMR sampling, respectively, to have enough replicates for the statistical analysis.

### **6.2.3 Glycogen analysis**

Rapid sampling from the PBRs for glycogen determination was performed as follows: about 5 ml of cell suspension from the vessel was harvested through a sampling port with a syringe into a 15 ml tube. For samples from the dark period the tubes were covered with aluminum foil. Aliquots of 2 ml cell suspension (technical duplicates for each PBR) were pelleted by centrifugation at 14,000 rpm and 4 °C for 5 min (in a pre-chilled centrifuge). The supernatant was removed carefully and the remaining wet pellet was stored at -20 °C for batch processing at a later time point. Glycogen was determined essentially as described before (266), employing the D-Fructose/D-Glucose assay kit (Megazyme) adapted for use in a 96-well plate reader. Cell pellets were re-suspended in 200 µl KOH (5.35 M) and hydrolyzed for 90 min at 95 °C in a thermomixer at 500 rpm. For glycogen precipitation, 600 µl of cold ethanol (absolute, Scharlau) were added to previously cooled samples and placed on ice for 2 hours. The insoluble glycogen was pelleted by centrifugation at 14,000 rpm at 4 °C for 5 min (in a pre-chilled centrifuge), and washed twice with cold ethanol. The remaining pellet was supplemented with 300 µl acetate buffer (200 mM, pH 5.2) and 50 µl amyloglucosidase (Roche) dissolved in acetate buffer and incubated overnight at 55 °C under constant agitation. Samples were centrifuged at 5,000 rpm at room temperature for 1 min and the glucose concentration was determined with the D-Fructose/D-Glucose assay kit (Megazyme) according to the manufacturers' instructions. The amount of glycogen was normalized to the gDW.

### **6.2.4 Dry cell weight measurements**

For the determination of the dry cell weight, for each PBR, two subsequent aliquots of 25 ml of the culture were harvested into the same 30 ml pre-weighed glass tubes. The cell suspensions were pelleted by centrifugation at 10,000 rpm at room temperature for 10 min. The supernatant was removed carefully without disturbing the pellets after which the cell pellets were dried overnight in a stove at 110 °C. The tubes were subsequently weighted.

### 6.2.5 HPLC analysis of supernatant samples

We analyzed the external medium of the culture for potentially excreted fermentation products. Given a total volume of 1 L for the culture in the PBRs, which has  $0.36 \pm 0.01$  gDW (Fig. 6.1C), then 5.1 % of this (the maximal difference in glycogen content of the cells, Fig. 6.1E) is 18 mg. Hence, 18 mg of a C6 compound (such as glucose, the building block of the polymer glycogen) could have been mobilized from the internal glycogen storage. If invested into a C6 excretion product (for example glucose) we could expect a concentration of 0.1 mM in the extracellular medium. However, in supernatant samples from the five time points, we did not detect any of the common fermentation products such as lactic acid, acetic acid, formic acid, etc.; all of which have a detection limit of 50  $\mu$ M on our HPLC system (data not shown). This was tested as follows: 1 ml supernatant samples were treated with 100  $\mu$ l of 35 % perchloric acid (Merck), incubation on ice for 10 min and neutralized with 50  $\mu$ l of 7 M KOH (Merck). After thorough mixing, the precipitate was removed by centrifugation for 2 min at 12,000 rpm and filtration (Sartorius Stedin Biotech, minisart SRP4, 0.45  $\mu$ m). Separation of organic acids and alcohols was achieved with a Rezex ROA-Organic Acid H+ (8 %) column (Phenomenex) at 45 °C using a flow of 0.5 ml/min. A refractive index detector (Jasco, RI-1530) and AZUR 4.5 Software (Datalys) was used for detection.

## 6.3 Results and Discussion

A multi-omics approach was used to characterize the cellular physiology of *Synechocystis* over a diel light cycle in quasi-steady-state. Such a quasi-steady-state, which refers to no change from cycle to cycle, was obtained by growing *Synechocystis* in a photobioreactor (PBR) with turbidostat control with 12 hours illumination and 12 hours darkness. The PBR enabled automatic acquisition of growth data through the integrated densitometer measuring optical density (OD) at 680 and 735 nm, as well as frequent sampling for glycogen content. For metabolite, transcriptome and proteome analysis (see Supplemental Material, Materials and Methods) as well as sampling for dry cell weight and protein content, we chose to focus sampling around the time point of the shift from the light period to the dark period. This was motivated by the findings of Kucho et al. (238), which indicated significant changes in gene expression (thus indicating hierarchical regulation) at the transition from subjective day to subjective night under continuous light conditions in an entrained culture.

### 6.3.1 Growth is dynamic and exclusive to the light period

The slopes in OD<sub>735</sub>, arising from growth in between the pump-intervals (compare Supplemental Material, Fig. S1), allow determination of the growth rate in the respective time windows (Fig. 6.1A). With the exception of some outliers, the growth rate varies between 0.015 and 0.030 h<sup>-1</sup> (which correspond to doubling times of ~40 and 20 h, respectively), following a distinct pattern over the light period. After the dark period and a lag phase without growth (Supplemental Material, Fig. S1), the first time window that allows growth rate determination shows a growth rate of ~0.020 h<sup>-1</sup>. The growth rate then

increases over the course of the light period, peaks early in the second half of the light period (~8 h after light onset) and decreases towards its end, at which point the growth rate has decreased to 0.015 h<sup>-1</sup>. Thus, the growth rate shows an ‘arc-like’ shape as a function of time in the 12 h light period, even though the light intensity and the OD<sub>735</sub> (and dry weight (DW)) are constant during this time (Fig. 6.1B and C). This dynamic growth rate is certainly expected for an experimental setup as presented for *Synechocystis* in e.g. Labiosa et al. (267), where a dimming schedule to simulate an actual diel cycle (achieved by sinusoidal illumination) was used. However, a similar pattern for the growth rate arises here, despite our use of square-wave light/dark cycles. Therefore, although we do not simulate light availability and intensity according to natural diel settings, we observe the same growth behavior suggesting that corresponding physiological parameters will be comparable to past studies. Similarly, though phase-advanced with respect to the growth rate, the OD<sub>680</sub>/OD<sub>735</sub> ratio, which is indicative of chlorophyll content, increases and subsequently decreases over the course of the day (Supplemental Material Fig. S2B). This oscillation can be explained by the circadian clock, which *Synechocystis* is equipped with (236, 237). We have recently shown this pattern of growth rate and chlorophyll content to also occur in an entrained culture in continuous light conditions (148).

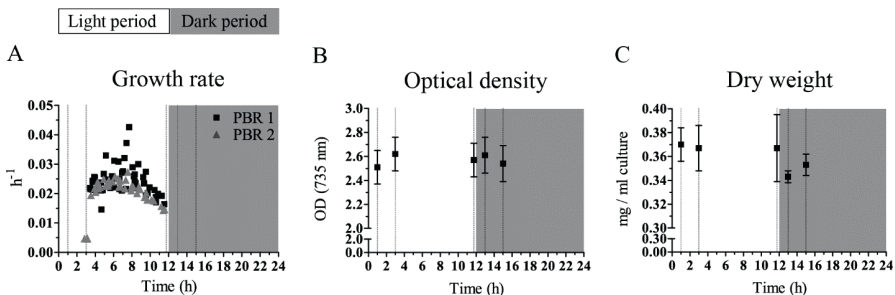


**Fig. 6.1.** Growth characteristics of a turbidostat-controlled culture treated with a repetitive diel light regime of 12 hours light and 12 hours dark. (A) Growth rates, calculated by linear regression of log-transformed OD<sub>735</sub>, changes during the growth phases in the light. Data from multiple days (1 week) for both PBRs are shown. Depending on the starting OD at the beginning of each light period, this results in 5 to 9 consecutive pumping/non-pumping intervals. The respective X-axis value is chosen from the end time point of the time window of the non-pumping interval. (B) Average optical density showing a stable signal at the dedicated sampling time points. (C) The cell dry weight shows a rather stable value. For all: dashed vertical lines represent the time points of sampling for dry weight, metabolite, protein and transcript analysis. For B: Values are the average and standard deviation derived from the biological replicates ( $n_{\text{biol}}=2$ ). For C: Values are the average and standard deviation derived from the biological replicates ( $n_{\text{biol}}=2$ ) and two technical replicates ( $n_{\text{tech}}=2$ ). Note the split Y-axes for B, and C.

### 6.3.2 Metabolite, proteome and transcript data place nitrogen and sulfur assimilation into the light period and indicate hierarchical regulation

To see whether the observed pattern of growth rates is reflected in the acquired omics data, we used statistical analysis to evaluate the different omics profiles. Multivariate data

analysis employing a supervised method, partial least square discriminant analysis (PLS-DA) of the metabolite signals from the 5 time points collected (in **Fig. 6.1**, the dashed vertical lines represent the time points of sampling), shows significant changes of the metabolite profile over the 24 hour period (Supplemental Material **Fig. S5**). Next, we aimed at finding proteins that change in time and share a biological function, annotated in the cyanobacterial sequence information repository Cyanobase (268). By performing ANOVA on the set of all quantified proteins (Supplemental Material, **Table S1**), we identified 45 proteins that showed a significant change in at least one of the five consecutive time points ( $p$ -value  $< 0.05$ ) (Supplemental Material, **Table S2**).

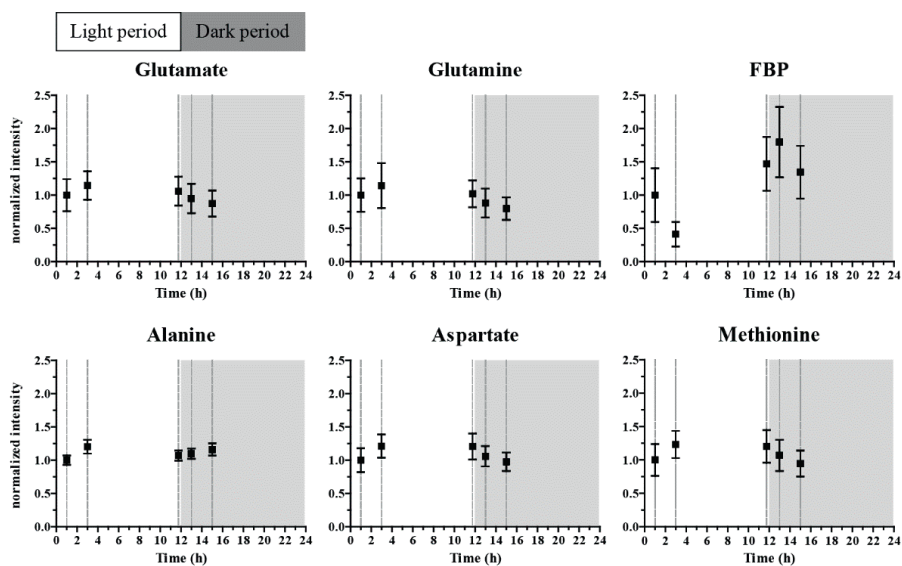


**Fig. 6.2.** Dynamically changing metabolites over the L/D cycle. Selected identified metabolites from the NMR analysis. Intensity values are normalized to the value of the first sampling time point in the light period. Mean and Standard Error of the Mean (SEM) are shown.

We refer to those 45 proteins as the changing proteins. The results from the enrichment analysis for a biological function of this set can be found in Supplemental Material **Table S3**. The ANOVA-based transcript analysis of the Microarray data revealed that approximately 56 % of the genes probed show a time-dependent change ( $p$ -value  $< 0.05$ ) (Supplemental Material, **Table S4**).

If both a metabolite and the corresponding enzyme change in parallel with its gene transcript, hierarchical control can be assumed, whereas if a metabolite changes without a change in the corresponding protein level, metabolic control can be assumed for the altered flux through the pathway under consideration. Based on the variable importance in the projection (VIP) scores (compare Supplemental Material, **Fig. S6** and **Table S5**) the metabolites that showed the largest changes were compared to the proteins involved in their respective metabolism, though the overlap between the metabolites identified

(Supplemental Material, **Table S5**) and proteins quantified (Supplemental Material, **Table S1**) is small. This comparison shows that from glutamate and glutamine metabolism, which are among the most dynamic metabolites in this study, two enzymes have been identified in the proteome analysis of this study: the glutamine synthases GlnA (Slr1756) and GlnN (Slr0288). GlnA is also present in the list of 45 changing proteins (Supplemental Material, **Table S2**, p-value 0.020) and its transcript is in the list of significantly changing genes (Supplemental Material, **Table S4**, p-value 0.007), showing strong downregulation in the dark (see entry *slr1756* in the Supplemental Material, **Table S4**). Inspection of the GlnA protein levels at the sampling time points shows that it decreases by ~20 % during the course of the light period and remains at the lower level in the dark period, whereas GlnN protein levels show no significant change (see entry Slr0288 in the Supplemental Material, **Table S1**). GlnN is mainly induced under nitrogen limiting conditions, explaining the low, stable levels observed (269). GlnA catalyzes the conversion reaction from glutamate to glutamine, thereby branching off intermediates from the TCA cycle. The down-regulation of both the GlnA protein levels and the transcript levels correlates with the trend of decreasing glutamine levels in the dark period and this enzyme might thus be regulated at least partially in a hierarchical fashion. However, glutamate shows reduced levels as well (**Fig. 6.2**), suggesting a generally lower influx into the glutamate and glutamine metabolism, implying that nitrogen assimilation takes place predominantly in the light.

In addition to glutamate and glutamine, methionine shows a similar pattern with higher levels in the light period (**Fig. 6.2**). This pattern is also reflected in aspartate, a precursor to methionine and part of cyanophycin, a known nitrogen storage compound. Methionine is one of the key amino acids through which sulfur is assimilated. When considering the machinery for sulfate reduction, it becomes apparent that this pathway is significantly downregulated in the night (*slr1165*, *slr0676*, *slr1791*,  $p < 0.05$ ) or shows no significant change (*slr0963*,  $p > 0.05$ , Supplemental Material, **Table S4**). The only protein of that particular pathway that was detected in our study, Slr0676, shows no significant change ( $p > 0.05$ ). Rather than concluding that this pattern is a general trend of synthesis of all amino acids, it should be noted that some other amino acids that were detected, e.g. glycine and threonine, do not show significant change over time and are among the lower scoring metabolites (VIP score  $< 1$ , Supplemental Material, **Table S5**). One metabolite that does change significantly over time, but does not mimic the trend displayed by the amino acids involved in nitrogen and sulfur assimilation, is alanine. This deviating pattern may stem from multiple pathways in which alanine is involved, such as transamination and, indirectly, glycolysis (270).

### 6.3.3 Integration of metabolite- and proteome data suggests metabolic control for the majority of the Calvin-Benson-Bassham cycle proteins

The list of most changing metabolites also contains fructose-1,6-bisphosphate (FBP) (Supplemental Material, **Table S5**). FBP shows lower levels at the early time points of the light period, followed by higher levels at later time points, even before the light period

ends and coinciding with reaching the maximal glycogen content (**Fig. 6.2**). FbaA, the FBP aldolase, participating in the Calvin-Benson-Bassham (CBB) cycle, is high at TP 1 and TP 2, and decreases to a lower level again in the three remaining sampling time points (**Fig. 6.3**), thus showing an opposite pattern to FBP (**Fig. 6.2**). FbaA also shows a significant time-dependent change determined by ANOVA ( $p$ -value  $2.0 \cdot 10^{-8}$ ), grouping it with the 45 changing proteins (Supplemental Material, **Table S2**). FBP is a part of both the CBB cycle and the glycolytic pathway (**Fig. 6.3**). The amount of Gap2, the prime glyceraldehyde-3-phosphate dehydrogenase in the fixation-direction of the CBB cycle is about 10-fold higher than the amount of Gap1, which, in turn, has been shown to be mainly active in glycolysis (271).

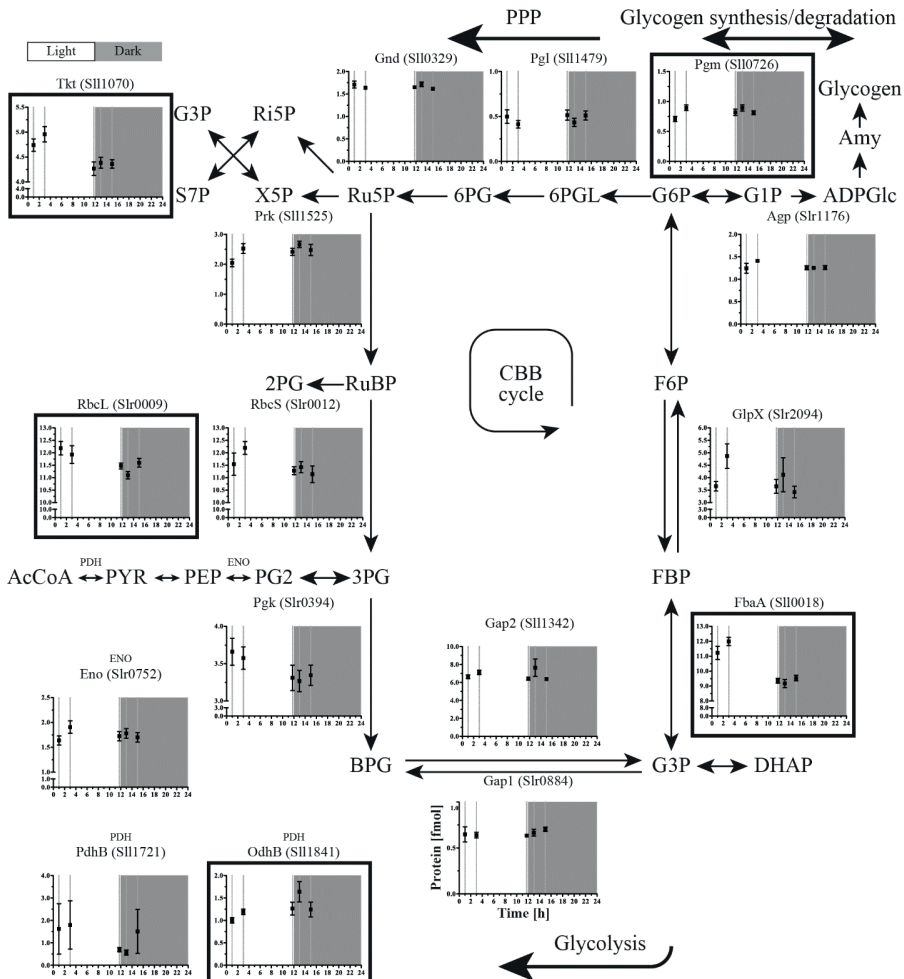


**Fig. 6.3.** Protein profiles of the CBB and central carbon metabolism. Those proteins that change significantly over time are marked with a black frame and are referred to as those that are subjected to hierarchical regulation. Mean and Standard Error of the Mean (SEM) are shown.

Both proteins seem to be kept at a rather stable level during the light/dark cycle that is imposed on the cells in this study. The enzyme catalyzing the preceding carbon-incorporating step in the CBB cycle, Ribulose-1,5-bisphosphate carboxylase/oxygenase (RuBisCO, RbcL and RbcS), shows slightly higher amounts during the early light period and a lower (~10 %) amount in the three remaining sampling time points, close to and in the dark period.

Of the CBB cycle (**Fig. 6.3**) next to FbaA, only RbcL (Slr0009) also appears in the list of changing proteins (p-value 0.024). The enzymes of the CBB cycle that are shared with the Pentose Phosphate Pathway (PPP) do not show a significantly altered pattern (**Fig. 6.3**). Nevertheless, the fluctuating FBP levels in concordance with the glycogen accumulation/degradation levels (see below) corroborate that the direction of the carbon flow through the regeneration phase of the CBB cycle, which overlaps with glycolysis, inverts between light and dark conditions (272) and here we show that this inversion of the direction of the flux only marginally makes use of hierarchical regulation of the participating enzymes (**Fig. 6.3**). In a recent study of Osanai et al. the transition from aerobic light to anaerobic dark conditions was investigated with a focus on metabolites (273). Of all metabolites investigated, exactly one overlaps with those that we identified here, which is FBP. Interestingly, and despite differences in experimental design, Osanai et al. also find relatively low FBP levels in the light and high levels under anaerobic dark conditions.

#### **6.3.4 Glycogen gradually accumulates in the light and is degraded in two distinct phases in the dark period**

Over the course of a diel cycle, the biomass composition of the cells is not as constant as the OD<sub>730</sub> and dry weight (compare **Fig. 6.1B** and **C**). Protein content (the soluble fraction, see Material and Methods for details) is higher in the early than the late light period and in the (early) dark period (**Fig. 6.4A**). An almost opposite pattern can be observed for the glycogen content of the cells (**Fig. 6.4B**). Glycogen is the main carbon storage compound of cyanobacteria (274, 275). Here, the glycogen content of the cells changes between 2.7 ± 1.0 % and 7.8 ± 0.4 % of the dry weight. Lowest levels of glycogen are present at the onset of the light period, but renewed accumulation starts immediately after the transition. In the 'afternoon' the glycogen level reaches a maximum and thereafter declines slightly during the rest of the remaining light period, as well as during the majority of the dark period.

Remarkably, ~2 h before the onset of the next light period, rapid glycogen degradation takes place, suggesting the investment of carbon into intracellular building blocks for the machinery supporting growth, to prime the cell for the upcoming light period. Based on flux balance analysis of a genome-wide model of the *Synechocystis* metabolism, Knoop et al. (276) calculate a linear degradation rate for glycogen over the majority of the dark period. Interestingly, that model further predicts that the glycogen content also decreases slightly faster during the last hours of the night.

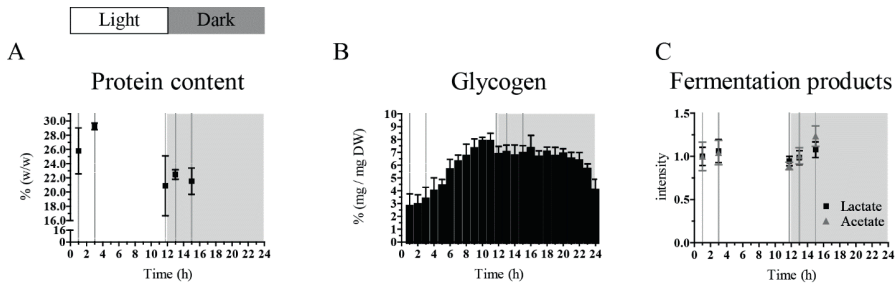


**Fig. 6.4.** Cellular composition of a turbidostat-controlled culture treated with a diel light regime of 12 hours light and 12 hours dark. (A) The protein content of the cells is higher at early time points of the light period compared to the later time point and the samples from the dark period. Values are expressed in % of dry weight (B) The glycogen content shows a distinct accumulation and degradation pattern. Values are expressed in % of dry weight (C) Metabolite analysis reveals a constant concentration of intracellular lactate and a slight increase for intracellular acetate in the early dark period. Intensity values are normalized to the value of the first sampling time point in the light period. For all: dashed vertical lines represent the time points of sampling for dry weight, metabolite, protein and transcript analysis. For A and B: Values are the average and standard deviation derived from the biological replicates ( $n_{\text{biol}}=2$ ) and two technical replicates ( $n_{\text{tech}}=2$ ). For C: Mean and Standard Error of the Mean (SEM) are shown. Note the split Y-axis for A.

The calculated flux through the participating enzymes in that flux balance analysis shows a higher flux through phosphoglucomutase (Pgm) exactly in the late dark period. Significantly, we do not detect any major fermentation product(s) in the extracellular medium (see Material and Methods for details).

Nevertheless, we do suggest that *Synechocystis* ferments in the dark and anoxic period, which leads to intracellular acetate and lactate formation. Interestingly, only acetate levels are increased 1 and 3 hours after the shift to the dark, whereas lactate levels remain constant over the five sampling points (**Fig. 6.4C**). This minimal fermentation activity is apparently not enough to support growth during the dark anoxic phase when respiration is not possible. We attribute the mild but gradual decrease in glycogen content during the majority of the dark period (before the rapid degradation sets in; see above) to its conversion into acetate. The energy yield of this conversion presumably covers the general costs of cellular maintenance during the dark period. It should be noted that this dark, anaerobic phase does not represent a major 'loss' of carbon. The carbon freed from glycogen during the slow degradation phase (i.e. 1.5 % (w/w) glycogen, between the maximum in the 'afternoon' and the time point just before the onset of the rapid degradation phase) corresponds to 0.0076 mmol carbon/gDW/h, taking glycogen as a C6 compound. This equals 0.1 nmol carbon/ (mg cell protein)/min, which is lower than the lowest reported rate of glycogen consumption in cyanobacteria by Stal and Moezelaar (265). This then also sets an upper limit to the maintenance requirements of the organism under anaerobic conditions in the dark of < 0.038 mmol ATP/gDW/h, assuming complete fermentation to acetate (265). Because of the acetate formation observed, it is likely that reduction of  $\text{H}^+$  or nitrate/nitrite is used to maintain redox balance. This is consistent with the strong upregulation (top 2-12 % of most-changing transcripts observed) in the dark of

the *hox* genes (*hoxEFUYH*, which are *sll1220*, *sll1221*, *sll1223*, *sll1224*, and *sll1226*) that encode the bidirectional NiFe-hydrogenase, as well as hydrogenase maturation gene *hypA1* (*slr1675*, top 1% of changing transcripts) (Supplemental Material, **Table S4**). Interestingly, the largest overall fold change is observed for *sll0741*, encoding the pyruvate flavodoxin/ferredoxin oxidoreductase which was recently shown to be the electron source of the hydrogenase (277). However, protein levels of ferredoxin-nitrite reductase remain stable whereas ferredoxin-nitrate reductase is not detected (Supplemental Material, **Table S1**). Furthermore, the transcript abundance indicates that nitrate/nitrite transport (*sll1450*, *sll1451*, *sll1452* and *sll1453*) and reduction (ferredoxin-nitrite reductase *slr0898* and ferredoxin-nitrate reductase *sll1454*) are downregulated in the dark (Supplemental Material, **Table S4**), which is consistent with our tentative conclusion that hydrogenase is the main redox valve in the dark (see above).

### 6.3.5 Consequences of square-wave diel cycles

The abrupt transition from dark to high light may cause high-light stress, as suggested by the lag phase in growth of ~2 hours. Proteome analysis revealed that significantly changing proteins are strongly enriched in the class of the ‘high-light and stress response proteins and chaperones’ (p-value < 0.005) (Supplemental Material, **Table S3**). Other indicators of stress are expression patterns of the orange carotenoid protein (OCP), superoxide dismutase (SodB) and the GroE chaperones (**Fig. 6.5**), which all show the highest levels at the beginning of the light period, coinciding with the lag phase before growth resumes (Supplemental Material, **Fig. S1**). Significantly, this high-light response was not evident in the gene-expression study of *Synechocystis* by Labiosa et al. (267), in which light intensity was gradually increased and decreased in time. In addition to the notion of possible initial high-light stress, the cells appear to experience constant high light during the light period. This follows from the detection of the high-light variant of the D1 protein, PsbA2, at all time points (see entries for Slr1311 in the Supplemental Material, **Table S1**). Furthermore, the *psbA2* (*slr1311*) and *psbA3* (*sll1867*) transcripts are both very abundant and are downregulated in the dark period whereas the *psbA1* (*slr1181*) transcript is weakly expressed and is upregulated in the dark period (compare Supplemental Material, **Table S4**). Accordingly, the significantly changing proteins are enriched in proteins of the category ‘photosystem II’ (Supplemental Material, **Table S3**). Additionally, the high-light transcript of the D2 gene, *psbD2* (*slr0927* in the Supplemental Material, **Table S4**) accumulates to similar levels as *psbD1* (*sll0849*). However, chlorophyll content, represented by the OD<sub>680</sub>/OD<sub>735</sub> ratio, actually increases in the first 3 h of the light period (Supplemental Material, **Fig. S2B**) and further increasing light intensity does not cause the typical photoinhibition phenotype of gradually reducing PSII activity, which would lead to decreasing oxygen evolution, indicating that the chosen conditions do not exceed the intrinsic photo-repair capacity (Supplemental Material, **Fig. S7**).

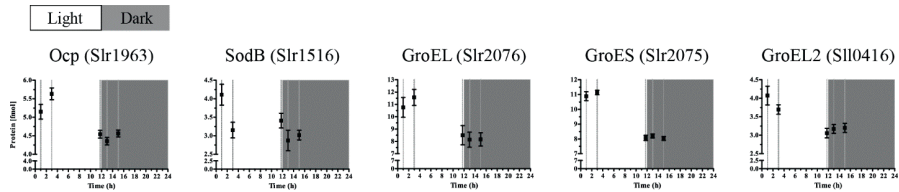


**Fig. 6.5.** High-light-response proteins and stress-response proteins show distinct changes at the onset of the light period. Mean and Standard Error of the Mean (SEM) are shown.

It is important to consider that the used light intensity does not surpass maximum light intensity at noon at moderate latitude and that cell density is high, leading to a steep gradient of light intensity within the culture and an actually fairly low light intensity per cell on average. This is emphasized by the low light transmittance of the culture (~5 % of incident light intensity) and lower oxygen evolution at the target density than at lower density.

Even though abrupt light-dark transitions do not reflect natural progression of light intensity over the course of a day, it facilitates discrimination of a direct light response from circadian regulation. We performed k-means clustering on the ANOVA filtered set of genes with  $k = 10$  to detect significantly differing time-dependent change (Supplemental Material, **Fig. S8**). K-means clustering on the set of the changing genes resulted in roughly two types with distinct patterns: the clusters 1, 5, 6 and 8 show upregulation upon the transition to the dark period whereas the clusters 2, 3, 4, 7, 9 and 10 show downregulation. However, cluster 7 is already downregulated before the transition whereas cluster 8 shows the opposite. In similar fashion, cluster 1 and 4 show a delay in up- or downregulation, respectively. Together, these four clusters represent 443 genes, or ~13 % of the total number of genes probed. Enrichment analysis on the ten clusters was done to identify significantly enriched functional categories for *Synechocystis*, based on Cyanobase (Supplemental Material, **Tables S8-9**). It is interesting to note that cluster 8 is enriched in genes involved in the PPP, despite clear downregulation of genes involved in RNA and DNA synthesis which are enriched in cluster 9.

For the set of changing proteins, k-means clustering resulted in four clusters with distinct patterns (Supplemental Material, **Fig. S9**). Two clusters, 2 and 4, show high levels in the early TPs, followed by a decrease during the light period and are both enriched in chaperones (Supplemental Material, **Table S10-11**). Cluster 3, on the other hand, shows its lowest levels around the end of the lag phase and is strongly enriched in proteins involved in photosynthesis and respiration. Cluster 1, despite appearing to correlate with light availability, is not significantly enriched in any biological category.

As mentioned above, most of the proteins detected show little or no changes over the five different time points of the light/dark regime. The proteins with very high p-values (above 0.8) from the ANOVA constitute the set of proteins which fail to show any evidence of time-dependent change at all. This prompted the identification of 19 proteins which we thus consider stable over time during the diel regime (Supplemental Material, **Table S6**).

An enrichment analysis based on the categories of the biological functions shows that phycobilisome proteins (p-value 0.006) are amongst these (Supplemental Material, **Table S7**). The phycobilisome proteins are the most abundant proteins found in the cells (278), which is corroborated by our analysis, and represent a major investment of resources for the cell, explaining their stable levels. It is interesting to note that the phycobilisome proteins show no change whereas the apparent chlorophyll content changes over the course of the light period in a similar fashion to a culture exposed to a much lower light intensity (Supplemental Material, **Fig. S2B**, (148)). We note that the MS-analysis and subsequent evaluation of the patterns of change were performed after normalization to the total soluble protein content.

## 6.4 Conclusion

Here, we show that *Synechocystis*, in a diel light regime with anaerobic conditions during the dark period, can grow only in the light and maintains a constant dry weight throughout the day. During the light period, glycogen accumulates as protein content decreases, and this reverses at the end of the dark period, restarting the daily cycle. Glycogen, assimilated during the day to a maximum of ~7.5 % of dry weight, is gradually fermented for maintenance requirements in the first 10 h of the dark period, followed by rapid degradation in the last 2 h. Nitrogen and sulfur assimilation take place predominantly in the light and hydrogen evolution is preferred over nitrate reduction during fermentation in the night. We conclude that maintenance costs are extremely low and require only a small fraction of the glycogen. The later rapid degradation of glycogen prepares the cells for growth in the upcoming light period, though a short lag phase is observed despite this priming of metabolism. Mass culturing under the conditions we have used in this study presumably will thus not be hampered by a huge 'loss' of carbon and energy in the dark period. The use of square-wave diel cycles allows for discriminating between circadian regulation and a direct light response. Our quantified proteome data set and the normalized transcriptome data set facilitate further investigation of potential proteins/genes of interest. The determination of their correlation will benefit the optimization of cyanobacterial production systems.

## 6.5 Acknowledgments

We are indebted to Naira Quintana (presently at Rousselot, Belgium) for the initiative to start the collaborative endeavor reported here. We are grateful to Timo Maarleveld from CWI/VU (Amsterdam) for a custom made Python™ script handling the output from the NMR analysis, and evaluating and visualizing the separate metabolites for their evaluation. We thank Rob Verpoorte from Leiden University (metabolome analysis) and Hans Aerts from the AMC (proteome analysis) for lab space and equipment. We are grateful to Robert Lehmann (Humboldt University Berlin) and Ilka Axmann (University of Düsseldorf) for sharing the R-code for the LOS transformation of the transcript data. We thank Hans Matthijs from IBED for inspiring dialogues and insightful thoughts on continuous culturing

of cyanobacteria. We are grateful to Sandra Waaijenborg for performing the transcript normalization and Johan Westerhuis from BDA, Jeroen van der Steen and Filipe Branco dos Santos from MMP and Lucas Stal from IBED/NIOZ for helpful discussions. We are very grateful to Milou Schuurmans from MMP for help with sampling and glycogen determination. We are further grateful to the members of the RNA Biology & Applied Bioinformatics group at SILS, in particular to Selina van Leeuwen, Elisa Hoekstra and Martijs Jonker, for the microarray analysis. We thank the reviewers of this work for their insightful comments which improved the quality of the manuscript. SAA, PvA, and KJH are supported by the research program of BioSolar Cells, co-financed by the Dutch Ministry of Economic Affairs, Agriculture and Innovation.